Rational Wiring of Photosystem II to Hierarchical Indium Tin Oxide Electrodes using Redox Polymers

Katarzyna P. Sokol,[1] Dirk Mersch,[1] Volker Hartmann,[2] Jenny Z. Zhang,[1] Marc Nowaczyk,[2] Matthias Rögner,[2] Adrian Ruff,[3] Wolfgang Schuhmann,[3] Nicolas Plumeré,[4,*] Erwin Reisner[1,*]

(1) Department of Chemistry, University of Cambridge, Lensfield Road, Cambridge CB2 1EW, UK

(2) Plant Biochemistry, Faculty of Biology & Biotechnology, Ruhr-Universität Bochum, Universitätsstr. 150, 44780 Bochum, Germany

(3) Analytical Chemistry - Center for Electrochemical Science (CES), Faculty of Chemistry and Biochemistry, Ruhr-Universität Bochum, Universitätsstr. 150, 44780 Bochum, Germany

(4) Center for Electrochemical Sciences (CES) - Molecular Nanostructures, Ruhr-Universität Bochum, Universitätsstr. 150, 44780 Bochum, Germany

*Corresponding authors: reisner@ch.cam.ac.uk; nicolas.plumere@rub.de

Abstract

Photosystem II (PSII) is a multi-subunit enzyme responsible for solar-driven water oxidation to release O_2 and highly reducing electrons during photosynthesis. The study of PSII in protein film photoelectrochemistry sheds light into its biological function and provides a blueprint for artificial water-splitting systems. However, the integration of macromolecules, such as PSII, into hybrid bio-electrodes is often plagued by poor electrical wiring between the protein guest and the material host. Here, we report a new benchmark PSII-electrode system that combines the efficient wiring afforded by redox-active polymers with the high loading provided by hierarchically-structured inverse opal indium tin oxide (IO-ITO) electrodes. Compared to flat electrodes, the hierarchical IO-ITO electrodes enabled up to an approximately 50-fold increase in the immobilisation of an Os-complex-based and a phenothiazine-based polymer. When the Os-complex-based polymer is co-adsorbed with PSII on the hierarchical electrodes, photocurrent densities of up to ~410 μA cm^{-2} at 0.5 V vs. SHE were observed in the absence of diffusional mediators, demonstrating a substantially improved wiring of PSII to the IO-ITO electrode with the redox polymer. The high photocurrent density allowed for the quantification of O_2 evolution, and a Faradaic efficiency of 85 ± 9% was measured. As such, we have demonstrated a high performing and fully integrated host-guest system with excellent electronic wiring and loading capacity. This assembly strategy may form the basis of all-integrated electrode designs for a wide range of biological and synthetic catalysts.

Introduction

The immobilisation of photosynthetic proteins onto electrodes is of importance to a range of current and future innovations, including biosensors,[1–3] biophotovoltaic systems[4–7] and photoelectrochemical (PEC) platforms.[8,9] Photosystem II (PSII) is a photosynthetic enzyme with the ability to photocatalyse water oxidation, a bottleneck reaction in artificial photosynthesis, at theoretical rates of up to 250 mol O_2 (mol PSII monomer)$^{-1}$ s^{-1}.[10,11] As such, there is considerable interest in the integration of PSII as a guest into electrode scaffolds,[12,13] in particular to improve our fundamental understanding of the protein function and also in PEC cells for proof of principle solar electricity/fuel generation.[14–17]

Several strategies for the integration of PSII into electrodes are currently employed, each with unique advantages. Before these approaches can be appreciated, some knowledge of the mechanism behind PSII water oxidation is required. Briefly, light is absorbed by pigments within PSII, and funnelled into the reaction centre complex where charge formation and separation at the P680 primary electron donor site occurs. The photogenerated electrons are then transferred via pheophytin and plastoquinone A (Q_A) to the terminal electron acceptor plastoquinone B (Q_B), which is located on the stromal side of the enzyme. Holes generated at the P680 are transferred in the lumenal direction, via a redox-active tyrosine side chain (Tyr_Z) to the oxygen-evolving complex (OEC), where water is oxidized to liberate H^+ and O_2.[18,19] If the PSII is adsorbed in the correct orientation on an electrode, direct electron transfer from the Q_A/Q_B to the electrode can take place.[20] However, a Q_B mimic, such as 2,6-dichloro-1,4-benzoquinone (DCBQ), is typically required as a diffusional mediator between the insufficiently wired PSII and the electrode to substantially enhance photocurrent generation.[19]

A traditional approach for the immobilisation of photosynthetic reaction centres is to align the proteins on chemically-modified electrodes functionalised with linkers such as quinonoid,[21] *N*-hydroxy-succinimidyl ester,[22] nickel nitrilotriacetic acid,[23,24] cytochrome c[25,26] and carboxylic acid/amino groups.[27] However, the magnitude of the photocurrent is limited by the attachment of a single monolayer of photosynthetic reactions centres that can be assembled on the electrode.

A strategy to enhance the loading of electrically wired PSII onto electrodes is to entrap PSII in a redox-active polymer matrix on an electrode surface.[28,29] In this approach, PSII of any orientation can in principle be efficiently wired to the electrode by the redox-active moieties that are homogeneously distributed in the matrix and mediate charge transfer via an electron hopping mechanism.[30] The benchmark system using this approach consists of a flat gold electrode on which PSII is embedded in an Os-complex-based polymer ($E_{1/2}$ = 0.395 - 0.505 V versus the standard hydrogen electrode; vs. SHE).[31] Photocurrents of up to 45 µA cm^{-2} at an applied potential of 0.5 V vs. SHE were reported for this biophotoanode. Despite its advantages, the performance of this system was limited by the intrinsic properties of the polymeric matrix. Independently of the total loading at the electrode surface, the amount of electroactive enzyme is defined by the rate of charge transfer via electron hopping, which limits the maximum (photo-)electrocatalytic response that can be detected.[32] On modified flat electrodes where enzymes are entrapped in redox polymers, the current generation typically arises from catalysts present within a thin layer (a few micrometer thick) at the electrode/hydrogel interface, and the remaining catalysts in the outer layers of the film are electro-inactive and do not contribute to current generation.[33]

An emerging and effective enzyme immobilisation strategy involves the adoption of highly structured electrode morphologies[34–36] to increase the available surface area for enzyme

adsorption.[9,27,37] In a recent benchmark system, PSII was adsorbed on a hierarchically-structured indium tin oxide (ITO) electrode that incorporated macroporosity (for enhanced enzyme and substrate penetration) and mesoporosity (to enhance the effective surface area and enzyme anchoring) with high thickness.[9] As a result, a 16,000-fold increase in PSII loading was observed compared to conventional flat electrodes.[6,31] However, insufficient wiring at the PSII-electrode interface was still apparent, with non-mediated photocurrents of 20 μA cm^{-2} being observed in contrast to 1 mA cm^{-2} being observed in the presence of a freely diffusing mediator. A further limitation of the electrode is poor PSII photostability, with the electrode exhibiting a photocurrent half-life of only a few minutes.

Here, we report a high performing PSII-electrode system that combines the best aspects of two advanced enzyme immobilisation strategies: the use of a redox polymer matrix to enable efficient PSII wiring, and the use of high surface area hierarchically-structured ITO electrodes to enable high loading of both the polymer and the PSII (Figure 1a). The highly structured electrode scaffold increases the polymer-electrode interface and reduces the average charge transfer distance between the PSII and the electrode surface via the polymeric matrix. This enables the wiring of a large population of PSII to the electrode, which translates to high effective loading. We first compared the performance of two promising redox polymers differing in chemical and redox properties as electron conducting matrices for PSII in inverse opal mesoporous ITO (IO-ITO) electrodes (Figure 1b). We then focused on the optimisation of the lead ITO-polymer-PSII system to ultimately deliver high photocurrents in the absence of diffusional mediators, at an extended operating half-life.

Experimental Section

Materials

All chemicals 1-vinylimidazole, 2,2'-bipyridine, allyl amine, K_2OsCl_6, butyl acrylate, allyl methacrylate, poly(ethylene glycol) methacrylate (M_n = 500 g mol^{-1}), 2,2′-azobis(2-methylpropionitrile) (AIBN), toluidine blue (all Sigma Aldrich), , DCBQ (Sigma Aldrich), 2-(N-morpholino)ethane sulfonic acid (MES, Alfa Aesar), $CaCl_2$ (Breckland Scientific), $MgCl_2$ (Fisher Scientific), KCl (Alfa Aesar), KOH (Breckland Scientific), NH_4OH (30%) solution (Fisher Scientific), H_2O_2 (30%) solution (Fisher Scientific), PS beads (Polysciences, Inc., 750 nm diameter, 2.6 % w/v suspension in H_2O), indium tin oxide (ITO) nanoparticles (NPs) (Sigma Aldrich; <50 nm diameter) and fluorine-doped tin oxide (FTO) coated glass slides (8 Ω cm^{-2}; Sigma Aldrich) were purchased from commercial suppliers and used without further purification unless otherwise noted. Methanol, absolute ethanol, 2-propanol, dimethyl sulfoxide (HPLC grade) were purchased from Sigma Aldrich. Poly(ethylene glycol) diglycidyl ether (PEGDGE) (Polyscience, USA) and 2,2'-(ethylenedioxy)diethanethiol) (Sigma Aldrich) were purchased from commercial suppliers. PSII was isolated from the thermophilic cyanobacterium *Thermosynechococcus elongatus* and purified according to a previously reported procedure,[38] resulting in purified PSII with an average oxygen-evolving activity of approximately 5,300 µmol O_2 h^{-1} mg^{-1} of chlorophyll *a* (Chl *a*). A stock PSII solution containing 2.6 mg Chl *a* mL^{-1} (83 µM PSII) was stored in a liquid N_2 Dewar.

Polymer synthesis

The synthetic approaches to obtain the P_{Os} backbone, the Os precursor *cis*-[$Os^{II}Cl_2(bipy)_2$] (bipy = 2,2'-bipyridine) and the Os complex *cis*-[Os^{II}Cl(1-(*n*-butyl)-imidazole)$(bipy)_2$](PF_6) were described previously.[31,39] The redox polymers poly(1-vinylimidazole) $Os(bipy)_2$Cl-polymer (P_{Os}),[31] and phenothiazine-modified polymer (P_{Phen}, phenothiazine moiety =

toluidine blue)[6] were synthesized according to previously reported procedures (for characterisation see Supporting Information), with P_{Os} prepared with slight modifications. In brief, after stirring a mixture of *cis*-[$OsCl_2(bipy)_2$] and the poly(1-vinylimidazole) backbone (1:1.65 weight ratio) dissolved in ethanol for 5 days at 90 °C, the final product (P_{Os}) was precipitated upon addition of diethyl ether. The precipitate was separated by centrifugation, thoroughly washed with diethyl ether and dried under vacuum to obtain a reddish powder. Aqueous stock solutions of P_{Os} (10 mg mL^{-1}) and P_{Phen} (10 mg mL^{-1}) were used.

Physical characterisation

The surface morphology of the electrodes was analysed by scanning electron microscopy (SEM; Philips SFEG XL30). A 5804 Eppendorf centrifuge and Carbolite furnace (ELF 11/14B/301) were used for electrode preparation. UV-vis absorption spectra were recorded on a Varian Cary 50 or Agilent Cary 60 UV-vis spectrophotometer, using cuvettes with an optical path length of 1 cm. Nuclear magnetic resonance (NMR) experiments were conducted with a Bruker 200 DPX spectrometer with a proton resonance frequency of 200.13 MHz (the residual solvent peak was used as internal standard). All dynamic light scattering (DLS) measurements were carried out with a Malvern Zetasizer Nano ZS (laser wavelength: 633 nm, measurement angle: 173° backscatter). The buffers were filtered through 450 nm membrane filters (polypropylene membranes bearing a borosilicate prefilter, Alltech) before dissolution of the polymers for DLS measurements; cuvettes were rinsed with buffer solution prior to measurements. For the filtration of polymer suspensions, non-pyrogenic 200 nm polyethersulfone PES-membranes (Filtropur S, Sarstedt) were used.

Preparation of IO-ITO|PSII electrodes

The IO-ITO electrodes were fabricated according to a previously reported procedure.[9] A standard IO-ITO electrode pore diameter of 750 nm, film thickness of 20 µm and geometrical surface area of 0.25 cm^2 were used, unless stated otherwise. An amount of 4.2 µL of the described polystyrene-ITO dispersion on a 0.25 cm^2 geometrical surface area corresponds to a 10 µm thick IO-ITO structure. To obtain higher film thicknesses, the polystyrene-ITO mixture (4.2 µL) was deposited several times with a 4 h drying period in between. All current densities (µA cm^{-2}) are reported with respect to the geometrical surface area. The IO-ITO|PSII modified electrodes were prepared as follows: a PSII stock solution (1 µL, 2.6 mg Chl *a* mL^{-1}) was drop-cast onto the IO-ITO electrode and incubated in the dark for 15 min at room temperature. It was determined that 1 µL of PSII stock solution provided an excess of PSII for 20 µm thick IO-ITO and ensured full enzyme coverage on the electrode surface. Prior to electrochemical studies, the IO-ITO|PSII electrode was rinsed (3 x 500 µL) with the electrolyte solution to remove all unbound enzyme from the electrode surface.

Preparation of IO-ITO|polymer-PSII electrodes

A PSII to polymer ratio of 1:1 (v/v) was defined based on 1 µL PSII stock solution (2.6 mg Chl *a* mL^{-1}) and 1 µL polymer solution (10 mg mL^{-1}). The PSII to polymer ratio was optimised on a 20 µm thick IO-ITO electrode by keeping the PSII solution volume (1 µL) and concentration (2.6 mg Chl *a* mL^{-1}) constant, and varying the polymer solution concentration at constant volume (1 µL). The optimal PSII to polymer ratio was found to be 1 µL of PSII solution (2.6 mg Chl *a* mL^{-1}) to 1 µL of the polymer solution (10 mg mL^{-1}) per 20 µm thickness of IO-ITO. The IO-ITO|polymer-PSII electrodes were prepared as follows: the PSII stock solution (1 µL) was mixed with a redox polymer solution (1 µL) and the polymer-PSII mixture was drop-cast (2 µL) onto the IO-ITO electrode (20 µm thick) and

incubated in the dark for 15 min at room temperature. Prior to electrochemical studies, the IO-ITO|polymer-PSII electrode was rinsed (3 x 500 µL) with the electrolyte solution.

Determination of PSII and polymer loading on IO-ITO

The amount of PSII on the IO-ITO surface was quantified by scratching off the IO-ITO from the glass substrate and washing with MeOH (500 µL) to extract Chl *a* from the electrode surface into a centrifuge vial. The vial was centrifuged (10,000 rpm, 1 min), and the UV-vis spectrum of the supernatant was recorded (Figure S6a). The band with an absorption maximum of λ_{max} = 665 nm assigned to Chl *a* (extinction coefficient ε = 79.95 (Chl *a* mg)$^{-1}$ mL cm^{-1})[40] was used to calculate the amount of PSII monomers assuming 35 Chl *a* molecules per PSII monomer.[41] The Os-complex loading in the P_{Os} polymer was determined by UV-vis spectroscopy, using the freely diffusing Os-complex analogue, *cis*-[Os^{II}Cl(1-(*n*-butyl)-imidazole)$(bipy)_2$](PF_6) for calibration, and confirmed by inductively-coupled plasma mass spectrometry (ICP-MS), obtained by washing off the P_{Os} from the IO-ITO electrode with aq. conc. HNO_3 solution and measuring the concentration of the Os^{2+} metal ions relative to Osmium ICP standard (1 mg Os mL^{-1} in 20% HCl, Ricca Chemical).

Protein film photoelectrochemistry (PF-PEC) measurements

All electrochemical experiments (except quantification of O_2) were performed with an Ivium Compactstat potentiostat with a purpose-built monochromatic red-light LED lamp (λ = 685 nm), collimated by two plano-convex lenses set (THORLABS N-BK7 A Coated, Ø= 7.5 cm, *f* = 5.0 cm). A light intensity flux (irradiance) (E_e) of 10 mW cm^{-2} was used, unless stated otherwise. Chronoamperometry and cyclic voltammetry (CV) measurements were carried out in a water-jacketed glass one-compartment cell at 25 °C with a three-electrode setup using an IO-ITO working, a Pt wire counter and a Ag/AgCl (3 M KCl) reference electrode. Measurements of the IO-ITO|polymer-PSII system were carried out in 4 mL aqueous pH

6.5 electrolyte solution containing $CaCl_2$ (20 mM), $MgCl_2$ (15mM), KCl (50mM) and MES (40 mM). For the mediated photocurrent measurements, a DCBQ solution in DMSO (40 µL, 100 mM) was added to give a final concentration of 1 mM in the electrolyte solution. The following correction factor was used to convert the reduction potential to SHE: $E_{SHE} = E_{Ag/AgCl} + 0.209$ V (25 °C). IO-ITO|polymer-PSII electrodes were typically exposed to cycles of 30 s dark and 30 s light irradiation in the PF-PEC measurements. The photocurrent response was defined as the baseline-corrected photocurrent peak after the third light exposure, accounting for charging effects and to avoid overestimation.[19] The action spectra were recorded using a Xenon lamp Solar Light Simulator (300 W) coupled to a monochromator (MSH300; both from LOT Quantum design). The light intensity was measured as a function of wavelength with a photodiode detector (SEL033/F/QNDS1/W) and power meter (ILT1400). For the O_2 evolution measurements, an Ivium Modulight LED module (λ = 660 nm; E_e = 10 mW cm^{-2}) and a gas-tight two-compartment glass cell with the IO-ITO|polymer-PSII working electrode separated from the counter electrode by a glass frit were employed in an anaerobic (O_2 level <1 ppm) MBraun glovebox. The error analysis was based on the standard deviations resulting from at least three experiments.

Product analysis

Quantification of O_2 was performed with a calibrated fluorescence O_2 sensor (Neofox; Ocean Optics FOSPHOR probe) inside an MBraun glovebox to avoid leakage of atmospheric O_2. The probe was placed inside the cell headspace, protected from direct irradiation and the background signal was subtracted from all measurements using the OriginPro 9.0 software. The reported O_2 values were corrected for dissolved O_2 using Henry's Law.

Equations 1 - 5:

$$\delta = \sqrt{\frac{D_e RT}{nF\nu}} \quad (1)^{42}$$

where δ - diffusion layer thickness of the electrons (m), D_e - apparent electron diffusion coefficient ($m^2\ s^{-1}$), R - ideal gas constant (8.314 J K^{-1} mol^{-1}), T - temperature (K), n - the number of electrons transferred, F - Faraday constant (96,485.332 C mol^{-1}) and v - scan rate ($V\ s^{-1}$).

$$\Gamma = \frac{Q}{nF\mathrm{A}} \quad (2)^{42}$$

where Γ - surface coverage of the electrochemically-active redox centres ($mol\ m^{-2}$), Q - total charge passed (C) and A - geometric electrode area (m^2).

$$\Gamma_{\mathrm{PSII}} = \frac{(16.29A^{665-750} - 8.54A^{652-750})\mathrm{V_{MeOH}} \times 10^6 g\ mL^{-1}}{35\mathrm{M_{Chl\ \mathit{a}}} \times \mathrm{A}} \quad (3)^{40}$$

where Γ_{PSII} - surface coverage of immobilised PSII ($mol\ m^{-2}$), A^{λ} - UV-vis absorption of Chl *a* at a given λ, V_{MeOH} - MeOH volume (mL) and $M_{Chl\ a}$ - molecular mass of Chl *a* (893.5 g mol^{-1}).

$$EQE = \frac{I_{\mathrm{e}}}{I_{\lambda}} = \frac{\frac{J}{F}}{\frac{\lambda E_{\mathrm{e}}}{N_A hc}} = \frac{hcJ}{e\lambda E_e} \quad (4)^{14}$$

where EQE - external quantum efficiency (defined as the number of incident photons converted to electrons at a selected irradiation wavelength), I_e - electron flux at the external circuit ($mol\ m^{-2}\ s^{-1}$), I_{λ} - incident photon flux ($mol\ m^{-2}\ s^{-1}$), h - Plank constant (6.626×10^{-34} J s), c - speed of light (3.00×10^8 m s^{-1}), J - photocurrent density ($A\ m^{-2}$), e - electron charge (1.602×10^{-19} C), N_A - Avogadro constant (6.022×10^{23} mol^{-1}), λ - irradiation wavelength (m) and E_e - light intensity flux (irradiance) ($W\ m^{-2}$).

$$\mathrm{TOF_{PSII}} = \frac{I}{4eN_A n_{PSII}} \quad (5)^{9}$$

where TOF_{PSII} - theoretical initial PSII-based O_2 evolution turnover frequency (assuming 100% Faradaic efficiency, except where O_2 was quantified) (mol O_2 (mol PSII)$^{-1}$ s^{-1}), *I* - photocurrent response (A) and n_{PSII} - amount of immobilised PSII (mol).

$$\mathrm{TON_{PSII}} = \frac{It}{4eN_A n_{PSII}} \quad (6)^{9}$$

where TON_{PSII} - theoretical PSII-based O_2 evolution turnover number (assuming 100% Faradaic efficiency, except where O_2 was quantified) (mol O_2 (mol PSII)$^{-1}$) and t - time (s).

Results and Discussion

Synthesis and characterisation of IO-ITO electrode and polymers

This study uses a hierarchical IO-ITO electrode, which has previously demonstrated a high loading capacity for large enzymes, such as PSII and hydrogenase (Figure S1a).[9] The macropores with diameter of 750 nm and channels of 150 nm are also suitable for the penetration of macromolecular polymers; the mesopores with a diameter of approximately 50 nm provide a high effective surface area of ~115 × 10^6 m^2 m^{-3} for polymer/enzyme adsorption.[9] The tunability of the film thickness (up to 80 μm, Figure S1d) provides extra flexibility in the optimisation of guest loading. The PSII used was isolated from the thermophilic cyanobacterium *Thermosynechococcus elongatus* given that cyanobacterial PSII is relatively well characterised,[41,43,44] and it exhibits high activity and robustness.[38,45]

The polymers chosen for this study include the P_{Os} (Figure 2a), which has demonstrated excellent integration of PSII on flat electrodes;[31] and the purely organic P_{Phen} (Figure 2b), which has a better matched redox potential with the Q_A/Q_B sites and has also demonstrated favourable wiring of PSII to flat electrodes.[6] Both polymers are compatible

with PSII and are stable under the acidic pH conditions for photocurrent measurements.[6,39] The chemical structure, purity and size of the polymers were confirmed by ^{1}H NMR (Figure S2), UV-vis spectroscopy (Figure S3) and dynamic light scattering (DLS, Figure S4), respectively. The ^{1}H NMR spectra of the polymer backbones correspond to the expected structure (Figure S2). Based on the integral ratio between methyl groups of terminal isopropyl units and the intra-chain imidazole unit, as well as the two signals assigned to the polymer chain, a molecular weight of ~26 ± 3 kDa was estimated for the P_{Os} backbone. For the backbone of the P_{Phen} polymer the analysis of the molecular weight via NMR spectroscopy was not possible due to overlapping signals in the spectrum of the backbone.

The total number of Os complexes in P_{Os} was quantified using UV-vis spectroscopy (0.74 ± 0.04 mmol g^{-1} polymer, Figure S3), which is consistent with ICP-MS measurements (0.67 ± 0.05 mmol Os g^{-1} polymer). *Cis*-[Os^{II}Cl(1-(*n*-butyl)-imidazole)$(bipy)_2$](PF_6) (Figure S3c), which can be regarded as the freely diffusing analogue to the Os-complex moiety in the P_{Os}, was used as a reference for characterisation by UV-vis spectroscopy. The spectrum of the freely diffusing complex and the polymer exhibit the same spectral features (Figure S3a). Thus, for the calculation of the total number of Os-complexes within the polymer, we assume that both species exhibit the same extinction coefficients. From the UV-vis studies, the ratio of non-complexed imidazole units to Os-complex moieties was calculated to be ≈ 7:1, which corresponds to a molecular weight of ~44 ± 5 kDa for P_{Os}. The same analysis was performed with the freely diffusing toluidine blue (Figure S3c) and P_{Phen}. The spectral shapes of both species are again similar (Figure S3d), but the extinction coefficient of the toluidine blue moiety is increased upon covalent attachment to the polymer backbone (the primary amine in the toluidine blue monomer is converted to a secondary or even to a tertiary amine upon reaction with the epoxide functionality of the

polymer backbone of P_{Phen}). Thus, the estimation of the exact number of toluidine blue species was not possible (calculated values exceed the theoretical values).

The hydrodynamic particle diameter of P_{Os} and P_{Phen} was determined using DLS (Figure S4) to be 16 ± 1 nm and ~500 nm (broad distribution), respectively, which indicate the agglomeration of smaller polymer chains. Since both polymer solutions were filtered through a membrane with 200 nm pore size, it was concluded that the P_{Phen} polymer chains form weak agglomerates that can be easily disassembled. The estimated sizes and agglomeration properties of P_{Os} and P_{Phen} are expected to allow them to enter into the IO-ITO structure either by diffusional transport or by convection due to the capillary forces induced by pore filling and H_2O evaporation.

Integration of PSII and polymer into IO-ITO electrodes

The polymers (1 µL, 10 mg mL^{-1}) were drop-cast onto the IO-ITO and allowed to adsorb for 15 min at room temperature. The redox properties of the adsorbed polymers on the IO-ITO electrode (IO-ITO|polymer) were characterised using cyclic voltammetry (CV; Figure 2c and Figure S5). The redox waves of P_{Os} and P_{Phen} were attributed to the $Os^{3+/2+}$ ($1e^-$ transfer process) and $Phen^+$/PhenH ($2e^-/H^+$ transfer) redox couples, respectively.[6] The positive reduction potential of the P_{Os} polymer ($E_{1/2}$ = 0.44 V vs. SHE) is expected to provide a large driving force for electron transfer from the Q_A and Q_B ($E_{1/2}$ = −0.14 V and −0.06 V vs. SHE, respectively) to the redox centres of the polymer (Figure 1b). However, electron transfer between Q_A/Q_B and the Os-complexes results also in a substantial potential loss (> 0.4 V).[5] The P_{Phen} hydrogel exhibits a more negative reduction potential ($E_{1/2}$ = 0.04 V vs. SHE), which matches the Q_B more closely (Figure 1b). The reversibility of the electron transfer process for the surface-adsorbed redox polymers is evident in the almost symmetrical shape in the CV scans of P_{Os} and P_{Phen}, which show minimal peak separation between the oxidation and reduction potentials (ΔE_p = 0.02 ± 0.01 and 0.01 ±

0.005 V for P_{Os} and P_{Phen}, respectively). Furthermore, an anodic to cathodic peak current ratio close to unity ($\frac{Ip_a}{Ip_c}$ = 0.97 and 0.83 for P_{Os} and P_{Phen}, respectively) can be observed, and the current density is linearly proportional to the scan rate up to 100 mV s^{-1} (Figure 2c inset and Figure S5).[42] The observed slight increase in the ΔE_p at scan rates >10 mV s^{-1} (Figure S5) was attributed to the rate limiting charge transfer between the polymer and the electrode surface.[46] In particular, P_{Phen} showed small shoulder waves at high scan rates that could arise from the slow $2e^-/H^+$ transfer rate at the iminium cation site. The voltammetric features of P_{Os}, even at the relatively fast scan rates used here, are characteristic for surface-confined species. The corresponding diffusion layer thicknesses of the electron (δ, calculated from Equation 1) give an estimate of the film thickness that is accessible to the electrochemical process assuming planar semi-infinite diffusion. Based on the previously reported apparent electron diffusion coefficient of the electron for P_{Os} (D_e of $(4.00 \pm 0.47) \times 10^{-9}$ $cm^2\,s^{-1}$)[39] the δ value corresponding to the scan rate of 100 mV s^{-1} is 320 nm. Hence, the diffusional range of the electrons within P_{Os} is in the range of the IO macropore radius (375 nm; Figure S1a) even at fast scan rates. As such, the IO structure should increase the total polymer loading that can participate in electron transfer in a given geometric surface area by taking advantage of the high thickness 3-D porous morphology.

No photocurrent originating from the IO-ITO|polymer electrodes during irradiation (λ = 685 nm, E_e = 10 mW cm^{-2}) was observed (Figure 2c). The surface coverage (Γ) of the electrochemically-active redox centres connected on the electrode surface was calculated for each polymer using Equation 2; the total charge was calculated by integrating the area under the CV curve minus the background. A substantial enhancement in polymer loading (Figure S5) was observed for IO-ITO compared to flat electrodes. The polymer loading increased approximately linearly with the electrode thickness (Figure 2d). Loadings of 1.7 ± 0.2 nmol cm^{-2} and 1.7 ± 0.5 nmol cm^{-2} were observed for flat ITO electrodes with the

adsorbed polymers, P_{Os} and P_{Phen}, respectively, which is comparable to previously reported values (1.8 ± 0.1 nmol cm^{-2}) on flat glassy carbon electrodes.[39] IO-ITO electrodes with a thickness of 20, 40 and 80 µm gave rise to a 15-, 23- and 45-fold increase in Γ_{Os} (25 ± 4, 38 ± 1 and 75 ± 3 nmol cm^{-2}) and 10-, 19- and 55-fold increase in Γ_{Phen} (17 ± 4, 34 ± 5 and 96 ± 16 nmol cm^{-2}) compared to a flat ITO electrode, respectively (Table S1). The number of electrochemically-active Os complexes on a 20 µm thick IO-ITO was found to be ~85 ± 10% of the total number of immobilised Os atoms, quantified by ICP-MS and UV-vis spectroscopy. The IO-ITO|P_{Os} electrode exhibited excellent stability, showing no significant desorption or decomposition after 100 CV cycles at 10 mV s^{-1} scan rate (Figure 2c). The IO-ITO|P_{Phen} electrode exhibited lower stability (63% and 38% Γ_{Phen} remaining after the second and third CV cycle at 10 mV s^{-1} scan rate, respectively, Figure S5e). The imidazole functionality in the P_{Os} is also likely to have a strong affinity for the ITO surface and act as an anchoring group, analogous to histidine-tagged enzymes.[47] The toluidine blue centres of the P_{Phen} (functional groups pK_a >7) are most likely deprotonated at pH 6.5. The hydrogel nature of the polymers allows the diffusion of small molecules throughout the network, although the lack of anchoring groups in P_{Phen} prevents stable loading.

Following the assembly and characterisation of the IO-ITO|P_{Os} and IO-ITO|P_{Phen} electrode systems, PSII was introduced into the electrode system. PSII (1 µL, 2.6 mg Chl *a* mL^{-1}) and the redox polymer (1 µL,10 mg mL^{-1}) were mixed together and immediately drop-cast on the IO-ITO electrode (20 µm thick) as a uniform blend, then allowed to adsorb in the dark for 15 min at room temperature. The amount of PSII entrapped in the polymer matrix inside the electrode (Γ_{PSII}) was quantified based on the absorption amplitude of Chl *a* (λ_{max} = 665 nm, Equation 3), extracted from PSII using MeOH (Figure S6a). UV-vis spectra of polymer solutions (0.02 mg mL^{-1}) in the electrolyte solution and MeOH (Figure S6b) showed a negligible absorption at the irradiation wavelength used in PF-PEC (λ = 685

nm). Exceptionally high PSII and polymer loadings were observed for IO-ITO|P_{Os}-PSII (144 ± 21 pmol cm^{-2}), IO-ITO|P_{Phen}-PSII (149 ± 7 pmol cm^{-2}) and IO-ITO|PSII (162 ± 17 pmol cm^{-2}) (Figure S6c). The slightly higher PSII loading in the PSII-only system could be justified by more space available that could be filled by the enzymes in the absence of polymers. The SEM images of the IO-ITO electrodes taken before (Figure S1a) and after P_{Os}-PSII and P_{Phen}-PSII deposition (Figure S1) indicate efficient electrode infiltration by the polymers with no channel or pore blockages.

The effective assembly of PSII with the polymers can be attributed to favourable non-covalent interactions between the protein shell and the polymers. The hydrophilic nature of the polymers is bestowed by the multiple polar functional side groups (P_{Os}: imidazole and amine groups; P_{Phen}: polyethylene glycol side chains and OH-functions), but mainly by the cationic Os complex/phenothiazine dye. At pH 6.5, P_{Os} is expected to behave as a cationic polyelectrolyte since the primary amine (pK_a 10) and imidazole groups (pK_a 7) are protonated. This also contributes to the close to optimal polymer solvation and swelling (with high D_e of (4.00 ± 0.47) × 10^{-9} cm^2 s^{-1}) previously observed.[39]

PF-PEC with IO-ITO|polymer-PSII electrodes

PF-PEC measurements were performed at 25 °C using an IO-ITO|polymer-PSII working electrode, a Pt wire counter electrode and a Ag/AgCl (3 M KCl) reference electrode. The electrolyte solution was adjusted to pH 6.5 and contained $CaCl_2$ (20 mM), $MgCl_2$ (15 mM), KCl (50 mM) and MES (40 mM). Action spectra of the IO-ITO|PSII, IO-ITO|P_{Os}-PSII and IO-ITO|P_{Phen}-PSII photoelectrodes were recorded to demonstrate which wavelength of light is most effective in photocurrent generation from PSII immobilised on the IO-ITO electrode (Figures 3 and S7). In a typical experiment, the wavelength was gradually decreased in steps of 20 nm starting from 760 nm at an applied potential of 0.5 V vs. SHE and the photocurrent response was measured at each wavelength. As anticipated,[48] the

maximum photocurrent was observed at 680 nm, which matches the UV-vis absorption spectrum of PSII and supports the integrity of PSII in its native state during the immobilisation on the IO-ITO electrodes.[21] The action spectra of the control samples IO-ITO, IO-ITO|P_{Os} and IO-ITO|P_{Phen} corresponded to the UV-vis absorption spectra of the respective polymers (Figure S6b) and confirmed no significant contribution to the photocurrent generation from the polymers (Figure S7).

Stepped chronoamperometry with chopped red-light irradiation (λ = 685 nm, E_e = 10 mW cm^{-2}) was performed to characterise the onset potential (E_{onset}) of photocurrents in each IO-ITO|polymer-PSII system (Figure S8). In a typical experiment, the applied potential was gradually increased in steps of 0.1 V in the anodic direction. A summary of the photoresponses as a function of the applied electrochemical potential (E_{app}) is shown in Figure 4. The IO-ITO|P_{Phen}-PSII system showed an E_{onset} value of ~0.1 V vs. SHE, which is more positive than expected due to the interference caused by other minor charge recombination pathways. However, the E_{onset} of IO-ITO|P_{Phen}-PSII is still clearly more negative than that of the IO-ITO|P_{Os}-PSII electrode (E_{onset} = ~0.3 V vs. SHE; Figure 4 inset), which is consistent with the lower $E_{1/2}$ of P_{Phen} ($E_{1/2}$ = 0.04 V vs. SHE) compared to the P_{Os} ($E_{1/2}$ = 0.44 V vs. SHE). The photocurrents for both the IO-ITO|P_{Os}-PSII and IO-ITO|P_{Phen}-PSII electrodes reach a plateau at ~0.5 V vs. SHE. No photoactivity and negligible dark current were observed for the IO-ITO|P_{Os} and IO-ITO|P_{Phen} electrodes (Figure S8d). Upon prolonged irradiation at more positive potentials (E_{app} > 0.6 - 0.7 V vs. SHE), a drop in photocurrent was observed. This drop in photocurrent is irreversible, as shown by the low photoresponse given by a backward scan in the negative direction (at 0.5 V vs. SHE, Figure S9a). CV scans of the IO-ITO|P_{Os}-PSII electrode (Figure S9b) confirmed the stability and homogeneity of the integrated PSII-polymer film on the electrode surface in the dark. However, CV scans

performed with red light irradiation (Figure S9c) show a significant decrease in photocurrents after 3 potential sweep cycles over the range 0.1 - 0.8 V vs SHE, which is indicative of P_{Os}-PSII film photodegradation (PSII-limiting system).[49]

To investigate the quality of the wiring between the PSII and the ITO electrode in the IO-ITO|polymer-PSII systems, chronoamperometry at an applied potential of 0.5 V vs. SHE was performed in the presence and absence of the diffusional mediator, DCBQ, with chopped light irradiation (Figure 5). Typical photocurrent densities for optimised 20 μm thick IO-ITO|PSII, IO-ITO|P_{Os}-PSII, and IO-ITO|P_{Phen}-PSII electrodes in the absence of a diffusional mediator (Figure 5a) were approximately 15, 230 and 45 μA cm^{-2}, respectively, which compares favourably with PF-PEC of previously reported PSII-electrodes.[9,19] Bare IO-ITO and IO-ITO|polymer electrodes exhibited photocurrent densities below 100 nA cm^{-2}.

The relatively large photoresponse observed for the IO-ITO|P_{os}-PSII system is indicative of efficient electronic communication between PSII and the electrode. An external quantum efficiency (EQE) of 4.4% (derived using Equation 4) was obtained for the IO-ITO|P_{Os}-PSII system, which is 15-fold higher than for IO-ITO|PSII (EQE = 0.3%) and the highest reported so far for a diffusional mediator-free PSII-electrode.[9,19] The photoresponse in the IO-ITO|P_{Phen}-PSII system (EQE = 0.8%) is improved compared to IO-ITO|PSII, however the enhancement is not as great as the IO-ITO|P_{Os}-PSII system, which indicates that the P_{Phen} is less efficient at wiring PSII to the electrode than P_{Os} possibly because of its significantly lower driving force for the electron transfer.

The addition of DCBQ (0.36 V vs. SHE)[9] to the IO-ITO|P_{Os}-PSII system gave rise to a further 1.5-fold photocurrent density increase (375 μA cm^{-2}, EQE = 7.7%, Figure 5b). Similarly, the addition of DCBQ to the IO-ITO|P_{Phen}-PSII system gave rise to a 6-fold photocurrent density increase (236 μA cm^{-2}, EQE = 4.6%). The addition of DCBQ to the

IO-ITO|PSII system gave rise to a much larger 18-fold increase in photoresponse (265 μA cm^{-2}, EQE = 5.1%). This observation demonstrates that a significantly higher proportion of PSII was electrochemically connected to the electrode in the IO-ITO|P_{Os}-PSII system than the IO-ITO|P_{Phen}-PSII system, and that the IO-ITO|polymer-PSII electrodes were better connected than the IO-ITO|PSII system. Addition of bifunctional cross-linkers (PEGDGE for P_{Os}[31] and 2,2'-(ethylenedioxy)diethanethiol for P_{Phen}[6]), to the IO-ITO|polymer-PSII systems resulted in no further photocurrent increase. This may be attributed to the stabilisation of the PSII-polymer matrix inside the 3-D-interconnected porous electrode framework.[9]

These results indicate favourable interactions between the P_{Os} and PSII, most likely between the side groups of the polymer (positively-charged Os^{3+} complex, primary amine and imidazolium units) and the polar residues of PSII,[41,50] in particular the negatively charged region at the stromal side of PSII and near the Q_A site.[37,51] In addition, a high number of electrochemically-active Os centres is estimated to be in close proximity to each PSII unit (based on the Os centre to PSII ratios ($\Gamma_{Os}/\Gamma_{PSII}$ ~175) co-adsorbed on the electrodes), which explains the good photoelectrochemical response of the system discussed earlier. The P_{Phen} can also interact with PSII via its hydrophilic side chains and residual epoxide groups to give rise to possible cross-linking.[41,50] However, the P_{Phen} is expected to have weaker interactions with the ITO electrode surface (Figure S5e), and is more likely to undergo polymer aggregation, as indicated by DLS, to result in significantly lower polymer entrapment and retention of PSII. The estimated number of toluidine blue units per PSII unit is 108, which is significantly lower than in the IO-ITO|P_{Os}-PSII system.

Comparison of P_{Os} and P_{Phen}

In the preceding experiments, PF-PEC was used to systematically compare the performance of two benchmark polymers for PSII entrapment when they are integrated

into high surface area electrodes. The P_{Os} exhibited the most stable integration in 20 μm thick IO-ITO electrodes. When embedded with PSII, the IO-ITO|P_{Os}-PSII electrodes delivered high photocurrent densities/TOF_{PSII} values that were at least 5-fold higher than systems connected by P_{Phen} (Figure 5a). Despite the fact that P_{Phen} is free of noble metals and has a better matched $E_{1/2}$ to the Q_A and Q_B (giving rise to earlier onset potentials for water oxidation), it exhibits lower adsorption stability on 20 μm thick IO-ITO electrodes. The IO-ITO|P_{Phen}-PSII systems showed lower overall photoresponses compared to IO-ITO|P_{Os}-PSII systems, which can also be justified by more negative redox potential (providing less driving force) and slower (H^+ diffusion-dependent) electron hopping process ($2e^-/H^+$ vs. $1e^-$ transfer, respectively). Overall, IO-ITO|P_{Os}-PSII electrodes demonstrated higher performance and more efficient wiring between the PSII and the ITO electrode.

IO-ITO|P_{Os}-PSII performance as a function of electrode thickness

To determine the enhancement of the photoresponse with film thickness in IO-ITO|polymer-PSII, IO-ITO electrodes which varied in thickness (from 20 to 80 μm) were prepared and studied by PF-PEC. The focus was placed on the optimisation of the best performing IO-ITO|P_{Os}-PSII systems.

The maximum loading of PSII and P_{Os} on IO-ITO electrodes of different thicknesses are shown in Figure 6a. The results show that P_{Os} and PSII loadings increase linearly as the thickness rises from 0 to 80 μm. In comparison, an adsorbent saturation point was reached for IO-ITO|P_{Os}-PSII electrodes beyond 40 μm. This was attributed to the formation of the P_{Os}-PSII complexes of high viscosity which show limited penetration depth in the thick IO structure. No significant losses due to desorption upon long-term (60 min) immersion in the electrolyte solution with constant light irradiation were observed.

The dependence of photocurrent density on the IO-ITO|P_{Os}-PSII electrode thickness is shown in Figure 6b. A saturation photocurrent density of 381 ± 31 μA cm^{-2} (EQE = 6.9 ± 0.9 %) for 40 μm thick electrodes was observed, which correlates with the maximum PSII loading reached at this thickness. Upon DCBQ addition, a further 1.35-fold photocurrent density increase was detected (513 ± 29 μA cm^{-2}, EQE = 9.3 ± 1.2 %). The IO-ITO|PSII electrode exhibited almost ideal linear increase in photocurrent densities with the ITO film thickness, which is also consistent with the trend of PSII loading in IO-ITO|PSII electrodes. Maximum photocurrent values of 33 ± 5 and 577 ± 21 μA cm^{-2} from 80 μm thick electrodes were observed in the absence and presence of DCBQ, respectively. The comparable maximum photocurrent densities reached by the IO-ITO|P_{Os}-PSII electrode in the absence of DCBQ and the IO-ITO|PSII electrode in the presence of DCBQ indicate excellent wiring of the PSII to the ITO surface by the P_{Os} matrix.

The theoretical TOF_{PSII} of water oxidation was estimated (assuming 100% Faradaic efficiency) according to Equation 5 for the IO-ITO|P_{Os}-PSII electrodes of different thicknesses as shown on Figure 6c. Maximum TOF_{PSII} of 4.0 ± 0.4 s^{-1} was achieved using 20 μm thick IO-ITO|P_{Os}-PSII electrodes, which could be increased to 6.7 ± 0.7 s^{-1} by the addition of DCBQ. This is a 1.7-fold increase compared to the IO-ITO|PSII system in the presence of DCBQ, and indicates that the mediated IO-ITO|P_{Os}-PSII system is overall more efficiently wired than the mediated IO-ITO|PSII system due to the presence of the P_{Os} matrix.

The long-term photostability of the IO-ITO|P_{Os}-PSII system was evaluated at a relatively mild E_{app} = 0.5 V vs. SHE and the results are presented in Figure 6d. To determine the photocurrent half-life time ($\tau_{1/2}$), the photocurrent generated by IO-ITO|P_{Os}-PSII electrode under continuous light irradiation for 60 min was recorded starting at the third photoresponse peak (Figure S10). Across the entire thickness range, the IO-ITO|P_{Os}-PSII

systems exhibited a 2-fold $\tau_{1/2}$ increase (maximum of 4.3 ± 0.4 min) compared to the IO-ITO|PSII systems (2.2 ± 0.2 min) in the absence of DCBQ. In the presence of DCBQ, further enhancement of the $\tau_{1/2}$ can be seen to reach ~10 min in 80 μm thick IO-ITO|P_{Os}-PSII electrodes. After 60 min of constant light irradiation, ~7% and 11% of the initial photocurrent was detected from the IO-ITO|P_{Os}-PSII electrode, without and with DCBQ addition, respectively. In contrast, less than 2% of the initial photocurrent was detected from the IO-ITO|PSII electrode. This can in part be attributed to the physical stabilisation of the PSII by the polymer matrix and the IO-ITO electrode architecture. The increased $\tau_{1/2}$ in the IO-ITO|P_{Os}-PSII system can also be partly attributed to reduced accumulation of pigments in the excited state due to more efficient electron transfer between PSII and the Os centres in P_{Os}.[49] The higher efficiency in charge transfer would result in dampened formation of reactive oxygen species and deterioration of D1 subunit in PSII.[52]

Finally, the photocurrent generated by the IO-ITO|P_{Os}-PSII electrode is high enough to enable the quantification of O_2 evolution for the first time with PSII in PF-PEC in the absence of a soluble diffusional mediator (Figure 7). Controlled potential electrolysis (CPE) at E_{app} = 0.5 V vs. SHE was carried out in a two-compartment cell in the glovebox employing an optimised 40 μm thick IO-ITO|P_{Os}-PSII electrode upon light irradiation for 60 min (λ = 660 nm, E_e = 10 mW cm^{-2}). The passage of 0.12 ± 0.03 C cm^{-2} charge was measured and the evolution of 0.24 ± 0.03 μmol O_2 cm^{-2} was detected by a fluorescence O_2 sensor, which corresponded to 85 ± 9% Faradaic efficiency. A turnover number TON_{PSII} of 946 ± 96 mol O_2 (mol PSII)$^{-1}$, and an initial PSII-based TOF_{PSII} of 3.6 ± 0.3 mol O_2 (mol PSII)$^{-1}$ s^{-1} was calculated based on quantified O_2 and PSII using Equations 6 and 5, respectively. Previously, the generation of 0.23 ± 0.01 C cm^{-2} charge and the evolution of 0.45 ± 0.01 μmol O_2 cm^{-2} (75 ± 4% Faradaic efficiency), corresponding to TON_{PSII} of 4200 ± 200 mol O_2 (mol PSII)$^{-1}$ and TOF_{PSII} of 12.9 ± 0.4 mol O_2 (mol PSII)$^{-1}$ s^{-1} were reported

for the IO-ITO|PSII system in the presence of DCBQ.[9] The PSII-based electrode here exhibits excellent performance without a diffusional mediator, which renders it a new benchmark PSII-electrode system. The absence of diffusion-limited mediators enables an all-integrated electrode design and eliminates problems such as those associated with concentration dependent electron transfer. It also overcomes the issue of diffusional mass transport that may interfere with processes at the counter electrode and limit the performance of PSII-based PEC assemblies. Lastly, it makes the new electrode prototype more applicable and interesting since all the catalytic/electroactive material is confined inside the porous electrode architecture and does not require the presence of large quantities in the bulk solution.

Conclusions

The present study has introduced a new benchmark PSII-based electrode, which was developed as a result of a rational design process that incorporated the best aspects of two leading enzyme immobilisation strategies. We integrated the stabilisation and efficient electronic wiring of enzymes within redox polymer matrices with the high loading capacity of hierarchically-structured electrodes. We demonstrate for the first time that high photocurrent densities, TOFs and levels of evolved O_2 could be obtained for a PSII-driven PF-PEC system without the requirement for diffusional additives in the bulk solution. The photocurrents arising from PSII reported here also compare favourably with those reported for other wired photosynthetic proteins such as bacterial reaction centres[53] or photosystem I.[4,39,54]

The development of the new IO-ITO|polymer-PSII system provides the basic concepts needed for the future design of enzyme-driven semi-artificial photosynthetic systems, including PEC tandem systems that incorporate other reaction centre or pigment-based

proteins. We anticipate that this approach will also serve as an inspiration for advancing the design of synthetic PEC water-splitting architectures. In the future, we expect that improvements in polymer design will lead to favourable changes to the electrode stability, enhanced electron hopping efficiency and formal redox potentials that exactly match the energy levels of the protein terminal electron acceptors. Lastly, hierarchical IO electrodes have demonstrated the potential to be highly versatile as a host system and may be used in various applications outside of PF-PEC, including batteries, fuel cells and solar cells.

Acknowledgements

This work was supported by the U.K. Engineering and Physical Sciences Research Council (EP/L015978/1 and EP/G037221/1, nanoDTC, and a DTA studentship to K.P.S.), the U.K. Biology and Biotechnological Sciences Research Council (BB/J000124/1), the Deutsch-Israelische Projektkooperation in the framework of the project “Nanoengineered optoelectronics with biomaterials and bioinspired assemblies”, the Cluster of Excellence RESOLV (EXC 1069) funded by the Deutsche Forschungsgemeinschaft (DFG), the COST Action TD1102 PHOTOTECH and a Marie Curie International Incoming Fellowship (PIIF-GA-2012-328085 RPSII to J.J.Z.). We would also like to thank Dr. Sascha Pöller and Ms. Sabine Alsaoub for their contributions to polymer synthesis, Dr. Julien Warnan, Mr. William Robinson, Dr. Bertrand Reuillard and Dr. Demetra Achilleos for valuable discussions and Mr. Wayne Bailey and Mr. Manuel Wentscher for building the monochromatic red-light LED lamp.

References

(1) Giardi, M. T.; Koblížek, M.; Masojídek, J. *Biosens. Bioelectron.* **2001**, *16*, 1027–1033.

(2) Koblížek, M.; Malý, J.; Masojídek, J.; Komenda, J.; Kučera, T.; Giardi, M. T.; Mattoo, A. K.; Pilloton, R. *Biotechnol. Bioeng.* **2002**, *78*, 110–116.

(3) Swainsbury, D. J. K.; Friebe, V. M.; Frese, R. N.; Jones, M. R. *Biosens. Bioelectron.* **2014**, *58*, 172–178.

(4) Mershin, A.; Matsumoto, K.; Kaiser, L.; Yu, D.; Vaughn, M.; Nazeeruddin, M. K.; Bruce, B. D.; Grätzel, M.; Zhang, S. *Sci. Rep.* **2012**, *2*, 1–7.

(5) Kothe, T.; Plumeré, N.; Badura, A.; Nowaczyk, M. M.; Guschin, D. A.; Rögner, M.; Schuhmann, W. *Angew. Chemie - Int. Ed.* **2013**, *52*, 14233–14236.

(6) Hartmann, V.; Kothe, T.; Pöller, S.; El-Mohsnawy, E.; Nowaczyk, M. M.; Plumeré, N.; Schuhmann, W.; Rögner, M. *Phys. Chem. Chem. Phys.* **2014**, *16*, 11936–11941.

(7) Nguyen, K.; Bruce, B. D. *Biochim. Biophys. Acta - Bioenerg.* **2014**, *1837*, 1553–1566.

(8) Yehezkeli, O.; Tel-Vered, R.; Michaeli, D.; Nechushtai, R.; Willner, I. *Small* **2013**, *9*, 2970–2978.

(9) Mersch, D.; Lee, C.-Y.; Zhang, J. Z.; Brinkert, K.; Fontecilla-Camps, J. C.; Rutherford, A. W.; Reisner, E. *J. Am. Chem. Soc.* **2015**, *137*, 8541–8549.

(10) Ananyev, G.; Dismukes, G. C. *Photosynth. Res.* **2005**, *84*, 355–365.

(11) Vinyard, D. J.; Ananyev, G. M.; Dismukes, C. G. *Annu. Rev. Biochem.* **2013**, *82*, 577–606.

(12) Tel-Vered, R.; Willner, I. *ChemElectroChem* **2014**, *1*, 1778–1797.

(13) Yehezkeli, O.; Tel-Vered, R.; Michaeli, D.; Willner, I.; Nechushtai, R. *Photosynth. Res.* **2014**, *120*, 71–85.

(14) Rao, K. K.; Hall, D. O.; Vlachopoulos, N.; Grätzel, M.; Evans, M. C. W.; Seibert, M. *J. Photochem. Photobiol. B* **1990**, *5*, 379–389.

(15) Badura, A.; Esper, B.; Ataka, K.; Grunwald, C.; Wöll, C.; Kuhlmann, J.; Heberle, J.; Rögner, M. *Photochem. Photobiol.* **2006**, *82*, 1385–1390.

(16) Terasaki, N.; Iwai, M.; Yamamoto, N.; Hiraga, T.; Yamada, S.; Inoue, Y. *Thin Solid Films* **2008**, *516*, 2553–2557.

(17) Yehezkeli, O.; Tel-Vered, R.; Wasserman, J.; Trifonov, A.; Michaeli, D.; Nechushtai, R.; Willner, I. *Nat. Commun.* **2012**, *3*, 742–748.

(18) Barber, J.; Tran, P. D. *J. R. Soc. Interface* **2013**, *10*, 20120984.

(19) Kato, M.; Zhang, J. Z.; Paul, N.; Reisner, E. *Chem. Soc. Rev.* **2014**, *43*, 6485–6497.

(20) Trammell, S. A.; Spano, A.; Price, R.; Lebedev, N. *Biosens. Bioelectron.* **2006**, *21*, 1023–1028.

(21) Katz, E. Y.; Shkuropatov, A. Y.; Vagabova, O. I.; Shuvalov, V. A. *Biochim. Biophys. Acta - Bioenerg.* **1989**, *976*, 121–128.

(22) Katz, E. *J. Electroanal. Chem.* **1994**, *365*, 157–164.

(23) Nakamura, C.; Hasegawa, M.; Yasuda, Y.; Miyake, J. *Appl. Biochem. Biotechnol.* **2000**, *84-86*, 401–408.

(24) Trammell, S. A.; Wang, L.; Zullo, J. M.; Shashidhar, R.; Lebedev, N. *Biosens. Bioelectron.* **2004**, *19*, 1649–1655.

(25) Lebedev, N.; Trammell, S. A.; Spano, A.; Lukashev, E.; Griva, I.; Schnur, J. *J. Am. Chem. Soc.* **2006**, *128*, 12044–12045.

(26) Yaghoubi, H.; Li, Z.; Jun, D.; Lafalce, E.; Jiang, X.; Schlaf, R.; Beatty, J. T.; Takshi, A. *J. Phys. Chem. C* **2014**, *118*, 23509–23518.

(27) Kato, M.; Cardona, T.; Rutherford, A. W.; Reisner, E. *J. Am. Chem. Soc.* **2013**, *135*, 10610–10613.

(28) Heller, A. *Curr. Opin. Chem. Biol.* **2006**, *10*, 664–672.

(29) Gracia, R.; Mecerreyes, D. *Polym. Chem.* **2013**, *4*, 2206–2214.

(30) Badura, A.; Kothe, T.; Schuhmann, W.; Rögner, M. *Energy Environ. Sci.* **2011**, *4*, 3263–3274.

(31) Badura, A.; Guschin, D.; Esper, B.; Kothe, T.; Neugebauer, S.; Schuhmann, W.; Rögner, M. *Electroanalysis* **2008**, *20*, 1043–1047.

(32) Bartlett, P. N.; Pratt, K. F. E. *J. Electroanal. Chem.* **1995**, *397*, 61–78.

(33) Fourmond, V.; Stapf, S.; Li, H.; Buesen, D.; Birrell, J.; Rüdiger, O.; Lubitz, W.; Schuhmann, W.; Plumeré, N.; Léger, C. *J. Am. Chem. Soc.* **2015**, *137*, 5494–5505.

(34) Li, Y.; Fu, Z.-Y.; Su, B.-L. *Adv. Funct. Mater.* **2012**, *22*, 4634–4667.

(35) Trogadas, P.; Ramani, V.; Strasser, P.; Fuller, T. F.; Coppens, M.-O. *Angew. Chemie Int. Ed.* **2015**, *54*, 2–29.

(36) Phillips, K. R.; England, G. T.; Sunny, S.; Shirman, E.; Shirman, T.; Vogel, N.; Aizenberg, J. *Chem. Soc. Rev.* **2016**, *45*, 281–322.

(37) Kato, M.; Cardona, T.; Rutherford, A. W.; Reisner, E. *J. Am. Chem. Soc.* **2012**, *134*, 8332–8335.

(38) Kuhl, H.; Kruip, J.; Seidler, A.; Krieger-Liszkay, A.; Bünker, M.; Bald, D.; Scheidig, A. J.; Rögner, M. *J. Biol. Chem.* **2000**, *275*, 20652–20659.

(39) Kothe, T.; Pöller, S.; Zhao, F.; Fortgang, P.; Rögner, M.; Schuhmann, W.; Plumeré, N. *Chem. - A Eur. J.* **2014**, *20*, 11029–11034.

(40) Porra, R. J.; Thompson, W. A.; Kriedemann, P. E. *Biochim. Biophys. Acta - Bioenerg.* **1989**, *975*, 384–394.

(41) Umena, Y.; Kawakami, K.; Shen, J.-R.; Kamiya, N. *Nature* **2011**, *473*, 55–60.

(42) Bard, A. J.; Faulkner, L. R. *Electrochemical Methods: Fundamentals and Applications*; Wiley: New York, 2001.

(43) Holzwarth, A. R.; Müller, M. G.; Reus, M.; Nowaczyk, M.; Sander, J.; Rögner, M. *Proc. Natl. Acad. Sci.* **2006**, *103*, 6895–6900.

(44) Rapatskiy, L.; Cox, N.; Savitsky, A.; Ames, W. M.; Sander, J.; Nowaczyk, M. M.; Rögner, M.; Boussac, A.; Neese, F.; Messinger, J.; Lubitz, W. *J. Am. Chem. Soc.* **2012**, *134*, 16619–16634.

(45) Kern, J.; Loll, B.; Lüneberg, C.; DiFiore, D.; Biesiadka, J.; Irrgang, K.-D.; Zouni, A. *Biochim. Biophys. Acta - Bioenerg.* **2005**, *1706*, 147–157.

(46) Laviron, E. *J. Electroanal. Chem. Interfacial Electrochem.* **1979**, *101*, 19–28.

(47) Lebedev, N.; Spano, A.; Trammell, S.; Griva, I.; Tsoi, S.; Schnur, J. M. *Org. Photovoltaics Viii* **2006**, *6370*, 63700T – 63700T11.

(48) Lai, Y.-H.; Kato, M.; Mersch, D.; Reisner, E. *Faraday Discuss.* **2014**, *176*, 199–211.

(49) Cai, P.; Feng, X.; Fei, J.; Li, G.; Li, J.; Huang, J.; Li, J. *Nanoscale* **2015**, *7*, 10908–10911.

(50) Suga, M.; Akita, F.; Hirata, K.; Ueno, G.; Murakami, H.; Nakajima, Y.; Shimizu, T.; Yamashita, K.; Yamamoto, M.; Ago, H.; Shen, J. *Nature* **2014**, *517*, 99–103.

(51) Khan, S.; Sun, J. S.; Brudvig, G. W. *J. Phys. Chem. B* **2015**, *119*, 7722–7728.

(52) Aro, E.-M.; Virgin, I.; Andersson, B. *Biochim. Biophys. Acta - Bioenerg.* **1993**, *1143*, 113–134.

(53) Friebe, V. M.; Delgado, J. D.; Swainsbury, D. J. K.; Gruber, J. M.; Chanaewa, A.; Van Grondelle, R.; Von Hauff, E.; Millo, D.; Jones, M. R.; Frese, R. N. *Adv. Funct. Mater.* **2016**, *26*, 285–292.

(54) Badura, A.; Guschin, D.; Kothe, T.; Kopczak, M. J.; Schuhmann, W.; Rögner, M. *Energy Environ. Sci.* **2011**, *4*, 2435–2440.

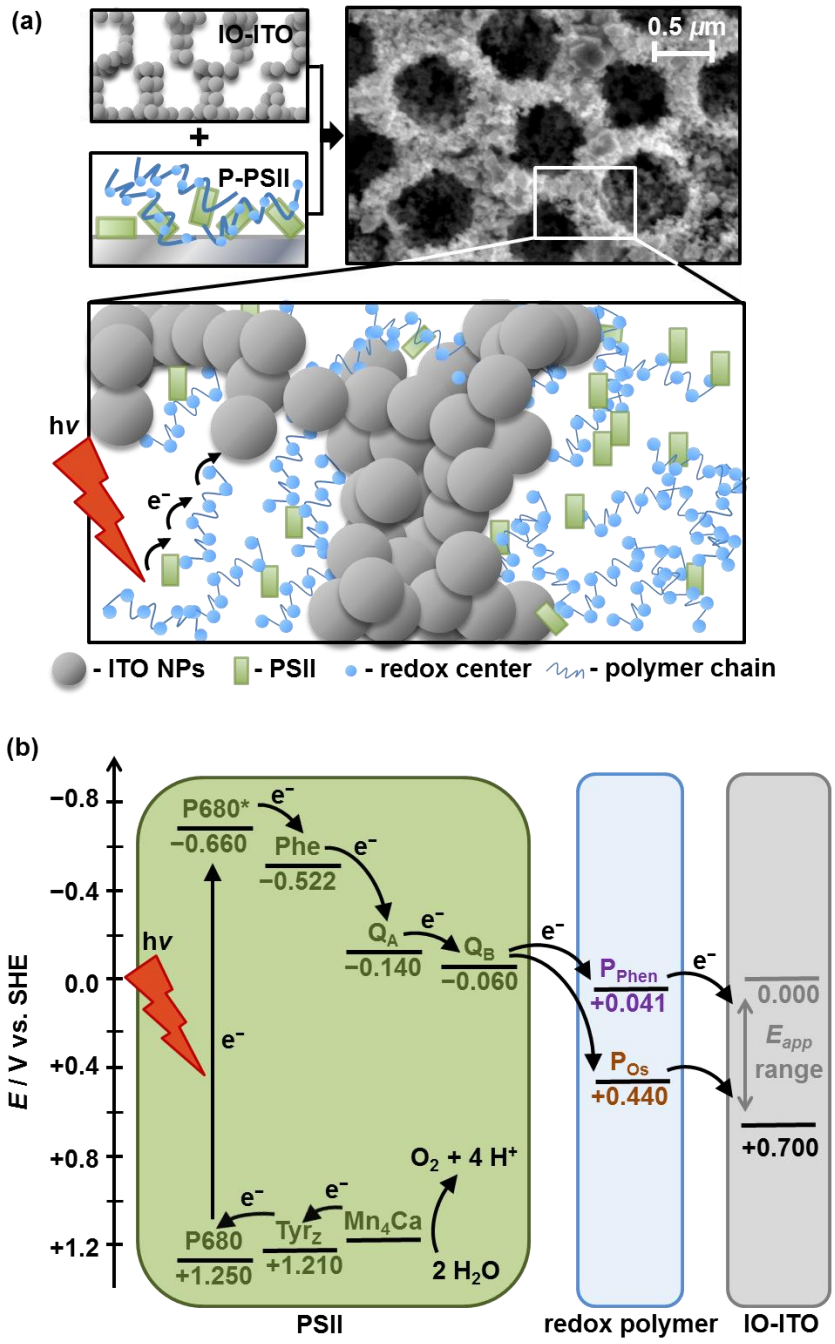

Figure 1. (a) Schematic representation and scanning electron microscopy (SEM) image of PSII wired via a redox polymer network to a hierarchically-structured IO-ITO electrode (species size not drawn to scale), indicating the electron transfer from photoexcited PSII to the electrode via the redox-active centres. (b) Energy level diagram showing electron transfer pathways between PSII, the redox polymer (P_{Phen} or P_{Os}, at pH 6.5) and the IO-ITO electrode (E_{app} refers to the applied electrochemical potential, which determines the Fermi level at the ITO electrode). Abbreviations: P680 - primary electron donor site, Phe - pheophytin, Q_A/Q_B - electron acceptor plastoquinones, Tyr_Z - tyrosine, Mn_4Ca - oxygen-evolving complex.

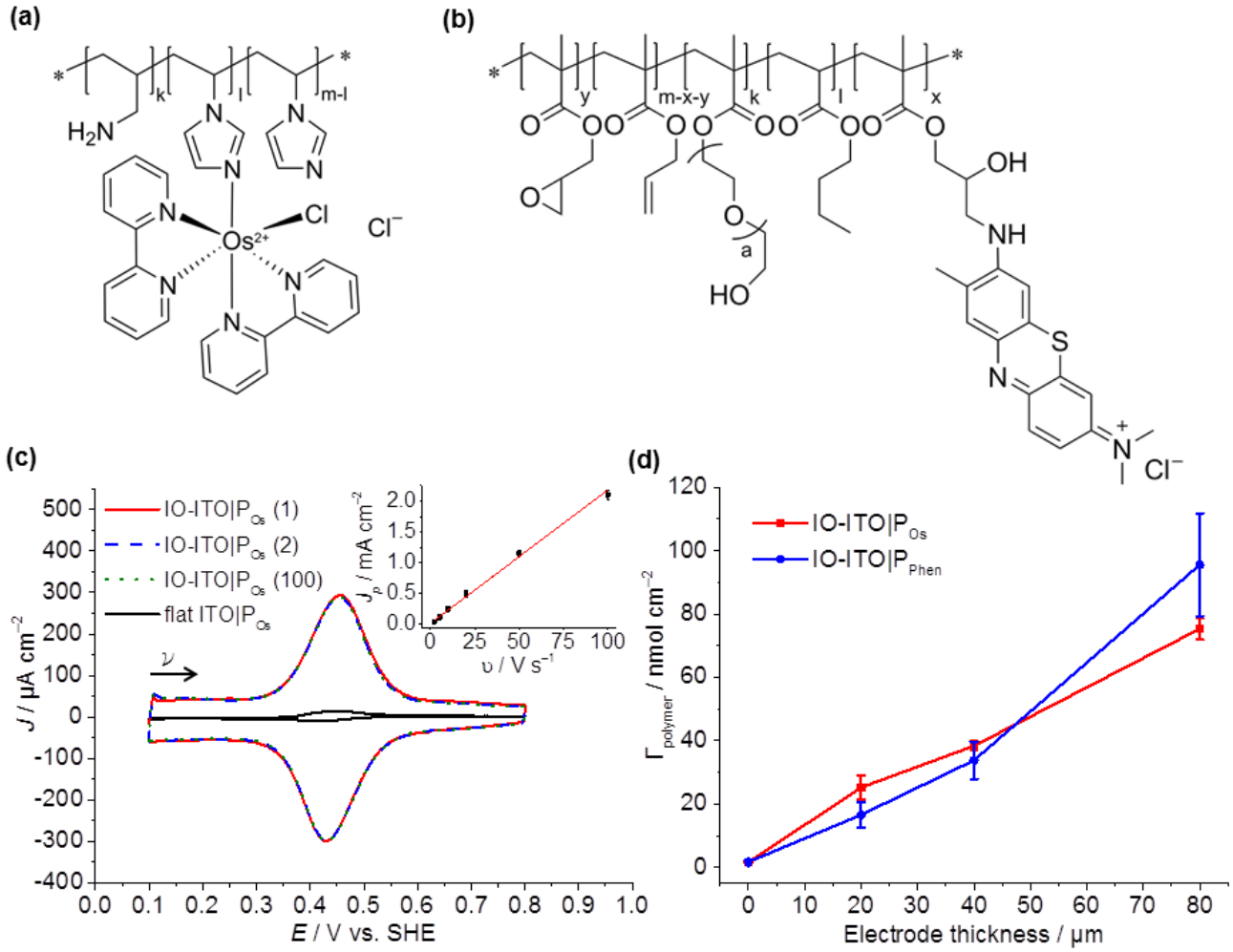

Figure 2. (a) Chemical structures of the P_{Os} and (b) P_{Phen} polymers. (c) CV scans of P_{Os} adsorbed on 20 μm thick IO-ITO (adsorbed 25 ± 4 nmol Os cm^{-2}) showing excellent stability on the electrode surface. The first scan and the 100th scan (dark, 10 mV s^{-1}) are shown by the red solid trace and the dark green dotted trace, respectively. The second scan was the only scan measured during irradiation (λ = 685 nm; E_e = 10 mW cm^{-2}), and is shown by the blue dashed line. A CV scan with P_{Os}-modified flat ITO (dark, 10 mV s^{-1}) is shown for comparison (adsorbed 1.7 ± 0.2 nmol Os cm^{-2}). The inset shows a linear dependence of the peak current density J_p with the scan rate v, confirming electron transfer of a surface-confined redox species. (d) Linear dependence of the redox-active centres loading for both polymers P_{Os} and P_{Phen} (up to 75 ± 3 and 96 ± 16 nmol cm^{-2}, respectively) with the electrode thickness confirms effective infiltration of the polymers into the electrode matrix. The error bars correspond to the standard deviation (N = 4). All experiments were carried out in a MES electrolyte solution (pH = 6.5, T = 25 °C).

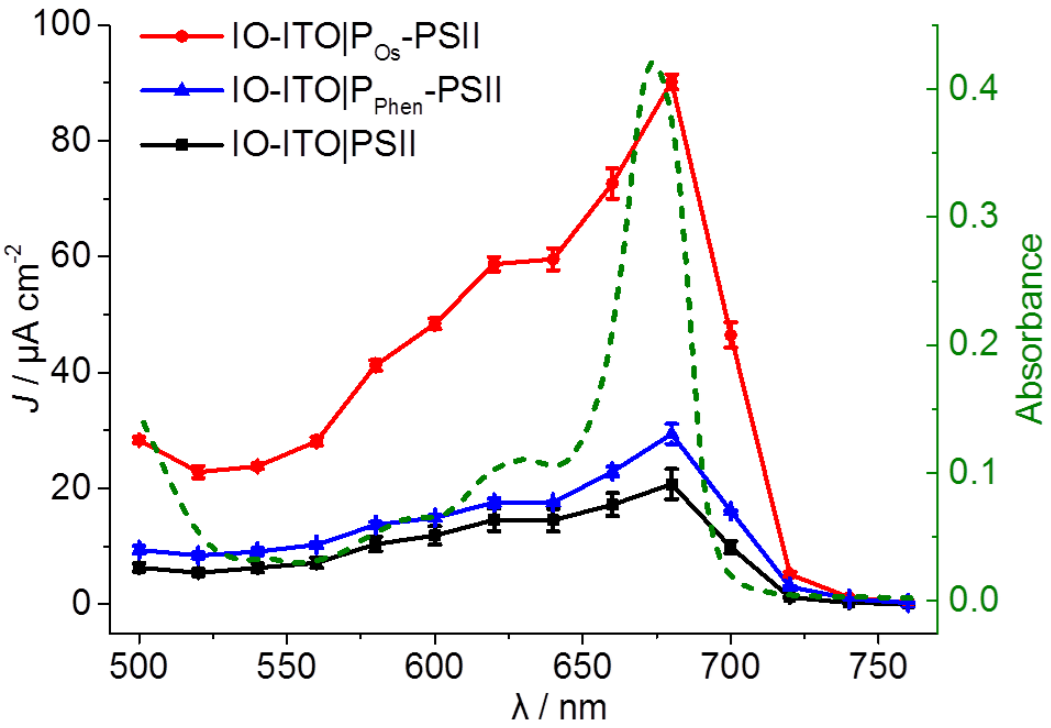

Figure 3. Action spectra (solid traces with left Y axis) showing the photocurrent density *vs*. irradiation wavelength of the IO-ITO|PSII (black), IO-ITO|P_{Os}-PSII (red) and IO-ITO|P_{Phen}-PSII (blue) photoelectrodes (20 µm thickness) recorded with monochromatic light measured in 20 nm steps (E_e = 3.25 to 6.26 mW cm^{-2}) at E_{app} = 0.5 V *vs*. SHE (pH = 6.5, T = 25 °C) in MES electrolyte solution (see Figure S7 for raw data and more detailed information). The error bars correspond to the standard deviation (N = 3). The UV-vis absorption spectrum of the PSII (1 µL, 2.6 mg Chl *a* mL^{-1}) in MES electrolyte solution (0.5 mL) (dashed green line with right Y axis) matches the photocurrent response of PSII on the electrodes.

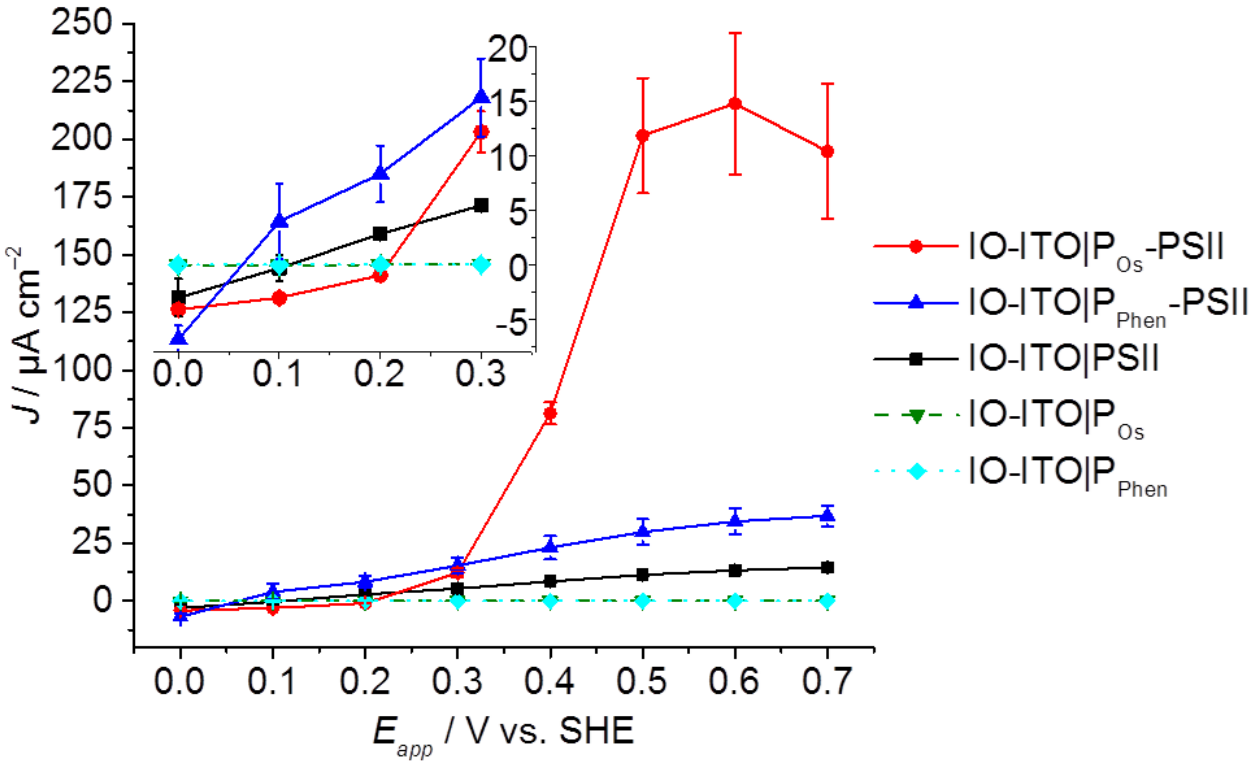

Figure 4. Photocurrent density as a function of the applied potential (E_{app}) for the IO-ITO|polymer-PSII photoanodes determined by stepped potential chronoamperometry (pH = 6.5, T = 25 °C) (see Figure S8 for raw data). The inset shows a magnified region of the plot close to the onset potentials of the polymers. The photoresponse for PSII-free IO-ITO|polymer electrodes are shown for comparison. The error bars correspond to the standard deviation (N = 4).

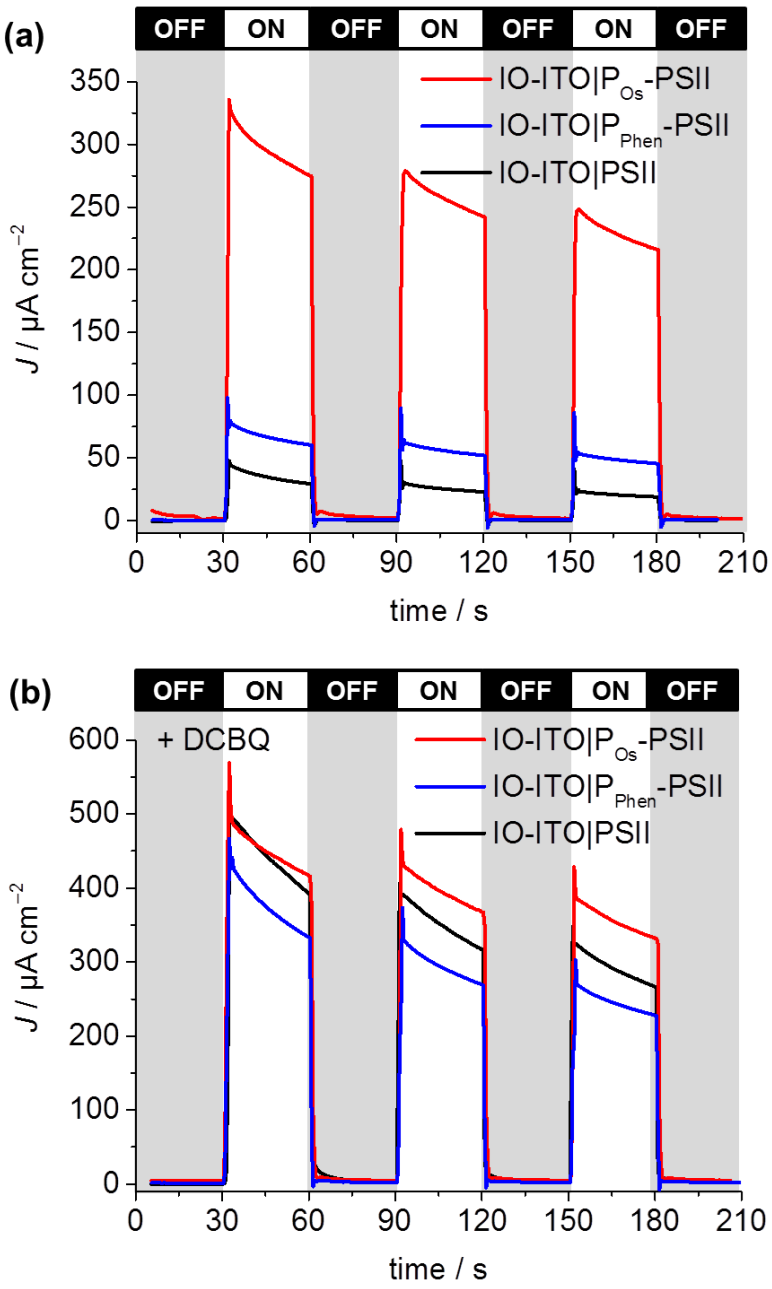

Figure 5. Photocurrent density of the IO-ITO|polymer-PSII and IO-ITO| PSII electrodes (20 µm thickness) measured with chopped illumination (λ = 685 nm; E_e = 10 mW cm^{-2}) at E_{app} = 0.5 V vs. SHE (pH = 6.5, T = 25°C). No diffusional mediator is present in (a) and DCBQ (1 mM) was present in the electrolyte solution in (b). The reported photocurrent densities were defined as the right shoulder of the third peak. The PSII loading for each modified electrode (see Figure S6) was comparable: 162 ± 17 pmol cm^{-2} (IO-ITO|PSII), 144 ± 21 pmol cm^{-2} (IO-ITO|P$_{Os}$-PSII) and 149 ± 7 pmol cm^{-2} (IO-ITO|P$_{Phen}$-PSII).

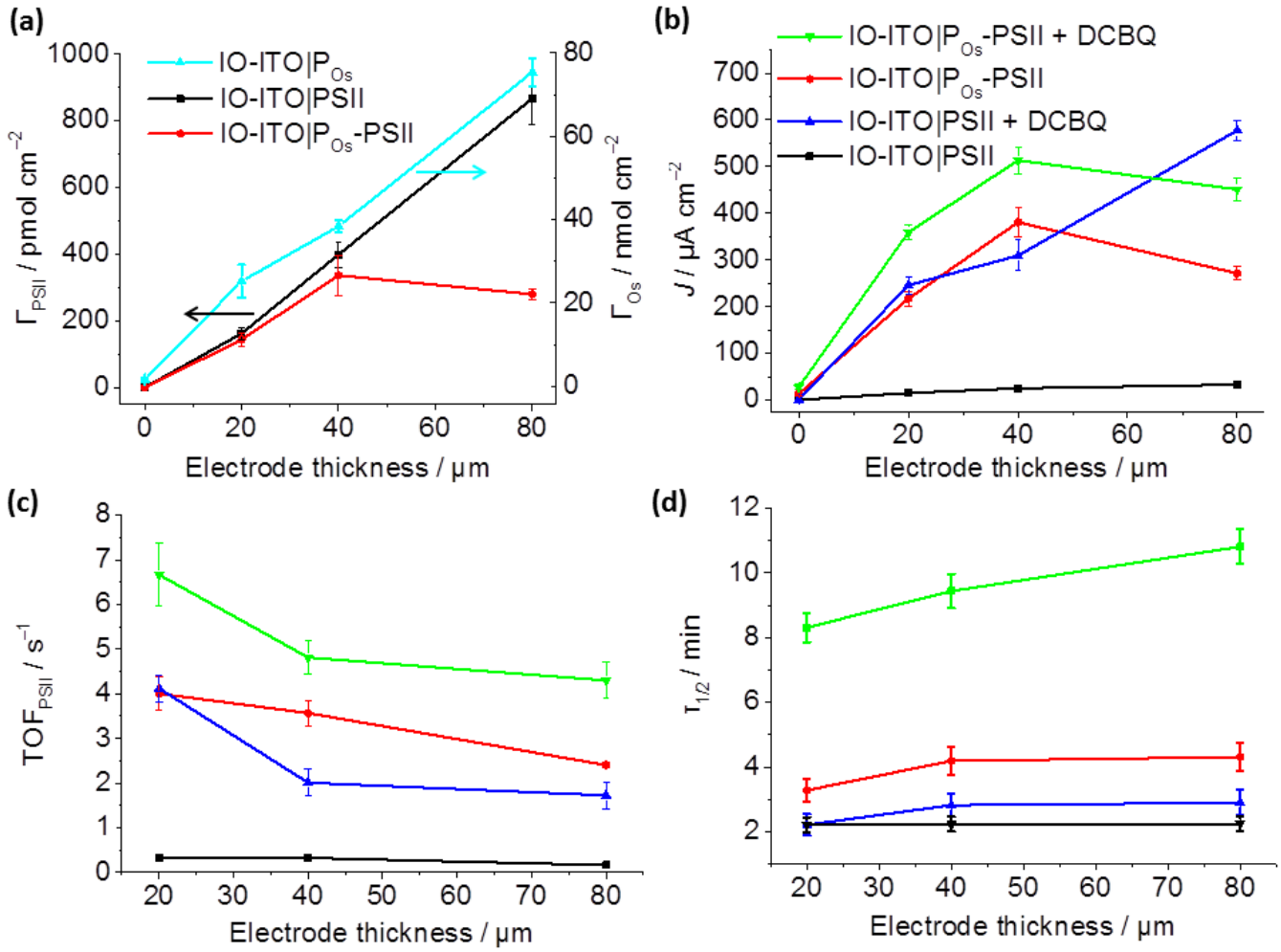

Figure 6. Characterisation of the IO-ITO|P_{Os}-PSII photoanode as a function of the electrode thickness: a) PSII loading quantified by the amplitude of absorption at λ = 665 nm, and $Os^{3/2+}$ redox centres loading determined by CV (Figure S5b); b) photocurrent densities, c) corresponding TOF_{PSII} values and d) photocurrent half-life times ($\tau_{1/2}$) measured upon light illumination (λ = 685 nm; E_e = 10 mW cm^{-2}) at a fixed potential of 0.5 V vs. SHE without any additional mediator and upon addition of 1 mM DCBQ mediator (pH = 6.5, T = 25 °C). The error bars correspond to the standard deviation (N = 4).

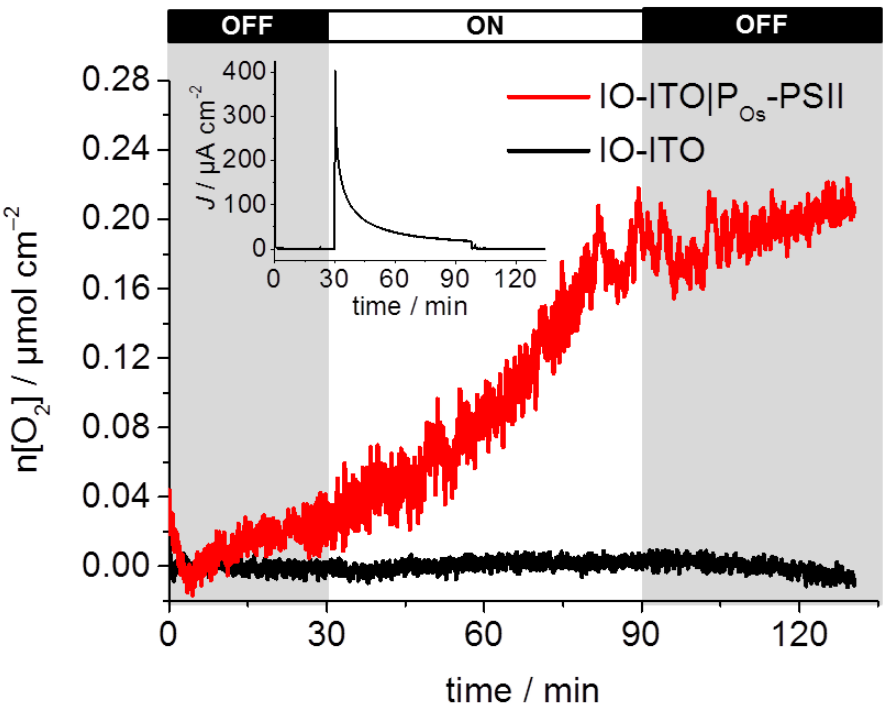

Figure 7. Quantification of O_2 evolution and determination of Faradaic yield (85 ± 9%) for the IO-ITO|P_{Os}-PSII electrode (40 µm thickness) during continuous light illumination (λ = 660 nm; E_e = 10 mW cm^{-2}) between 30 and 90 min with continuous stirring at E_{app} = 0.5 V vs. SHE (pH = 6.5, T = 25 °C, red line). The chronoamperogram is shown in the inset. A control experiment in the absence of PSII is also shown (black curve).

Table of Contents Artwork

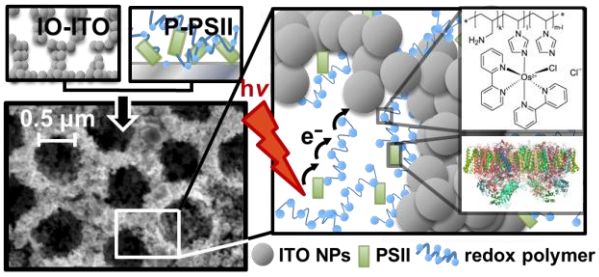

Broader Context

In natural photosynthesis, solar energy drives the conversion of CO_2 and H_2O into chemical energy carriers and building blocks and the release of O_2 as a by-product. Artificial photosynthesis attempts to mimic this process to produce a renewable and storable fuel. Photosystem II (PSII), the first protein complex in oxygenic photosynthesis, is capable of harnessing solar energy required to perform photocatalytic water oxidation, a bottleneck in artificial photosynthesis. As such, there is a substantial interest in integrating PSII onto electrode scaffolds to gain better insight into fundamental protein function and also in protein film photoelectrochemical (PF-PEC) platforms for proof of principle solar electricity and solar fuel generation. Here, we describe a novel rational approach for a PSII-based electrode assembly, where we electrically wired PSII using a redox polymer matrix onto high surface area electrode scaffold by combining two advanced enzyme immobilisation strategies. The PSII-polymer mixture integrated in a hierarchical indium tin oxide electrode provides the basis for high performance PSII-photoelectrochemistry and will by relevant for future enzyme-driven semi-artificial photosynthetic systems.